SANDIA REPORT

SAND 2003-3785
Unlimited Release
Printed October 2003

Equations of State for Titanium and Ti6A14V Alloy

Author(s)Gerald I. Kerley

Prepared by
Sandia National Laboratories
Albuquerque, New Mexico 87185 and Livermore, California 94550

Sandia is a multiprogram laboratory operated by Sandia Corporation,
a Lockheed Martin Company, for the United States Department of Energy's
National Nuclear Security Administration under Contract DE-AC04-94AL85000.

Issued by Sandia National Laboratories, operated for the United States Department of Energy by Sandia Corporation.

Available to DOE and DOE contractors from
U.S. Department of Energy
Office of Scientific and Technical Information
P.O. Box 62
Oak Ridge, TN 37831

Telephone: (865)576-8401
Facsimile: (865)576-5728
E-Mail: reports@adonis.osti.gov
Online ordering: http://www.doe.gov/bridge

Available to the public from
U.S. Department of Commerce
National Technical Information Service
5285 Port Royal Rd
Springfield, VA 22161

Telephone: (800)553-6847
Facsimile: (703)605-6900
E-Mail: orders@ntis.fedworld.gov
Online order: http://www.ntis.gov/help/ordermethods.asp?loc=7-4-0#online

SAND2003-3785
Unlimited Release
Printed October 2003

Equations of State for Titanium and Ti6Al4V Alloy

Gerald I. Kerley, Consultant
Kerley Technical Services
P.O. Box 709
Appomattox, VA 24522-0709

Abstract

The PANDA code is used to build tabular equations of state (EOS) for titanium and the alloy Ti4Al6V. Each EOS includes solid-solid phase transitions, melting, vaporization, and thermal electronic excitation. Separate EOS tables are constructed for the solid and fluid phases, and the PANDA phase transition model is used to construct a single multiphase table. The model explains a number of interesting features seen in the Hugoniot data, including an anomalous increase in shock velocity, recently observed near 200 GPa in Ti6Al4V. These new EOS tables are available for use with the CTH code and other hydrocodes that access the CTH database.

Acknowledgements

Sandia is a multiprogram laboratory operated by Sandia Corporation, a Lockheed Martin Company, for the United States Department of Energy's National Nuclear Security Administration under Contract DE-AC04-94AL85000. I am grateful to Sandia for supporting this work. I especially appreciate the efforts of Gene Hertel in the production of this report.

Contents

Figures

Tables

Symbols and Units

ρ	density [g/cm^3]
V	specific volume, $V = 1/\rho$ [cm^3/g]
T	temperature [K]
P	pressure [GPa]
E	specific internal energy [MJ/kg]
A	Helmholtz free energy [MJ/kg]
S	entropy [$MJ/(kg\text{-}K)$]
β	isothermal bulk modulus, $\beta = \rho(\partial P/\partial\rho)_T$ [GPa]
C_S	sound velocity [km/s]
U_S	shock velocity [km/s]
u_P	particle velocity [km/s]
R	gas constant [8.31451×10^{-3} $MJ/kg\text{-}mole\text{-}K$]
W	atomic or molecular weight [$g/mole$]
k	Boltzmann's constant [1.38066×10^{-29} MJ/K]

1. Introduction

Sandia National Laboratories (SNL) maintains an equation of state (EOS) database for use with the three-dimensional hydrodynamics code CTH [2]-[4]. This database includes default parameters for a number of materials and for several EOS models that are described in Refs. [5][6]. The present study is part of a continuing effort to evaluate and improve this database [7]-[14].

This report describes new EOS tables for titanium and its important alloy Ti6Al4V. The tables were constructed with the PANDA code [15], using a model that includes solid-solid phase transitions, melting, vaporization, and thermal electronic excitation. The approach is similar to that discussed in Refs. [10]-[14]; separate EOS were first constructed for each phase, and the PANDA phase transition model was used to create a single multiphase table including the transitions.

Titanium has an interesting phase diagram. It has been studied extensively, in both static and shock wave experiments and in theoretical calculations. Five solid phases—α, β, ω, γ, and δ—have been identified [16]-[19]. α, which has the hcp structure, is the stable phase at room temperature and pressure (RTP). β, which has the bcc structure, is formed at zero pressure and high temperatures (>1166K). ω, which has a distorted hexagonal structure, is formed on compression to 9-10 GPa at room temperature; this phase is also metastable on release back to zero pressure [20]. Melting occurs at 1941K.

The other two Group IV transition metals—Zr and Hf—have phase diagrams similar to that of Ti. Since Zr and Hf both transform from the ω phase to the β phase at high pressures [21][22], it was expected that Ti would exhibit the same behavior [23][24]. Instead, recent measurements showed that Ti transformed from ω to γ (distorted hcp) at 120 GPa and from γ to δ (distorted bcc) at 140 GPa [18][19].

A number of shock wave studies have shown that the ω phase is also formed on shock compression, at 10-11 GPa [25]-[27]. The transition splits the shock into two waves at pressures in the neighborhood of the transition. The ω phase can even be retained on release, if the samples are cooled before shocking [25]. Consideration of the phase diagram shows that the Hugoniot also traverses the β phase before crossing the melting curve; examination of the Hugoniot data does indicate a transition near 60 GPa.

The phase diagram of Ti6Al4V alloy is not as well known. However, it has been established that the alloy does *not* transform to the ω phase when shocked. Shock experiments similar to those for pure titanium did not show any evidence of splitting of the shock or any retention of the ω phase on release [27]. In addition, the shock velocity-particle velocity curve for the alloy lies above that for pure titani-

um at pressures above 10 GPa. The Hugoniot does exhibit evidence of a phase transition near 40 GPa, but the volume change is less than the transitions seen in pure titanium.

The EOS model for pure Ti is discussed in Sec. 2. The model development parallels that described in Ref. [13]. However, three solid phases are included instead of only one, leading to a more complicated phase diagram. Good agreement is obtained with thermophysical data, static measurements, and Hugoniot data, including measurements on highly porous materials.

The EOS model for Ti6Al4V is discussed in Sec. 3. This model uses the same basic formulas as for pure Ti, but the ω phase is omitted. The parameters for the zero-Kelvin isotherms are computed using additive volume mixing of the pure Ti phases with Al and V. The model predicts a stiffer Hugoniot for the alloy, in agreement with the data. The model also predicts a large jump in shock velocity near 200 GPa, due to melting, that is consistent with recent Hugoniot measurements.

Conclusions and recommendations are discussed in Sec. 4.

Appendix A gives plots of the tension region for the two materials.

2. Pure Titanium

2.1 Model Overview

Our model for pure titanium includes four phases—α, β, ω, and the fluid (including liquid, vapor, and supercritical regions). The γ and δ phases were treated as high-pressure extensions of the β phase, as discussed below. Separate EOS tables were constructed for each phase, using a common energy zero (α-Ti at RTP). The phase transition option was then used to construct a single multiphase table.

The EOS model for each phase is essentially the same as that previously used for Be, Ni, W, and Au [13]. A detailed description of the formulas is given in Ref. [13], and only the most important points are discussed here.

The model for the solid phase uses the Birch-Murnaghan formula for the zero-Kelvin isotherm and the Debye model for the lattice vibrations. The solid parameters were chosen to fit the following data: density [20][28][29], enthalpy and entropy [30], static compression [19][31][32], and Hugoniot [33]-[37]. Band-theoretical calculations of Ostanin and Trubitsin [24] were also considered in making the fits.

The CRIS model for the fluid phase uses a zero-Kelvin isotherm, similar to those for the solid phases, along with thermodynamic perturbation theory [38][39]. Additional parameters are used to define the solid isotherm in tension and to match the thermodynamic state of the liquid at the melting point.

The solid and fluid EOS also include the contribution from thermal electronic excitation and ionization. This term was computed by merging calculations from two quantum-statistical theories—the PANDA ionization equilibrium model at densities below the metal-insulator transition, and a modified version of the INFERNO model [13][40] at higher densities.

2.2 Solid Phases

The zero-Kelvin isotherms were fit to the Birch-Murnaghan (BM) equation ,

$$P_c(\rho) = \frac{3}{2}\beta_0(\eta^{7/3} - \eta^{5/3})\left[1 + \frac{3}{4}(\eta^{2/3} - 1)(\beta'_0 - 4)\right], \quad (1)$$

where $\eta = \rho/\rho_0$, and ρ_0, β_0, and β'_0 are constants. To insure correct asymptotic behavior at high densities, the PANDA extrapolation formula, which is based on Thomas-Fermi-Dirac (TFD) theory, was used at pressures above about 100 GPa (match density RTFD).

As we will show below, the Hugoniot for Ti traverses all three of the solid phases. In fixing the parameters β_0 and β'_0 for each phase, special emphasis was given to matching the Hugoniot in the appropriate pressure range. The parameters for ω and β were also constrained by the ω–β phase boundary.

Recent static measurements at 298K show that the ω phase transforms first to γ, then to δ, in the pressure range 124-145 GPa [19]. Our model, like that of Ostanin and Trubitsin [24], predicts the ω–β transition temperature to decrease at high pressures. In the absence of any other phases, the model predicts a transition from ω to β at room temperature and high pressure, as observed in Zr [21] and Hf [22]. Since existing data are insufficient to construct separate EOS for the γ and δ phases, we have treated them as extensions of the β phase. A tabular isotherm for the β phase was constructed from two sets of BM parameters—the Hugoniot fit below 124 GPa and the fit of Akahama, et al. [19], above 145 GPa, with an interpolation in the intermediate region.

In Ref. [13], the density dependence of the Grüneisen function Γ was computed from the generalized Dugdale-MacDonald option. This option is not suitable for use with the tabular isotherm because it uses both first and second deriviatives of the pressure. Therefore, the following expression was used in this work.

$$\Gamma(\rho) = \Gamma_{ref}/\eta + 0.5(1 - 1/\eta)^2, \eta = \rho/\rho_{ref}, \quad (2)$$

where ρ_{ref} is the density at RTP. The RTP Grüneisen parameter Γ_{ref} and Debye temperature Θ_{ref} for the α and β phases were obtained by fitting thermal expansion, sound speed, enthalpy, and entropy data. No thermophysical data are available for the ω phase. However, the fact that the α–ω phase boundary is nearly independent of temperature indicates that the thermal properties for the two phases are quite close. Therefore, the Grüneisen parameter and Debye temperature for ω were taken to be the same as for α.

The EOS table for each solid phase was set to give its heat of formation, $\Delta_f H^0$, at RTP. This condition guarantees a common energy zero for use in the phase transition model. The heat of formation was chosen to match the α–β transition temperature at zero pressure and the α–ω transition stress on the Hugoniot.

Table 1 lists eight parameters for each solid phase—the RTP density, the three BM constants, the TFD match density, the RTP Grüneisen parameter and Debye temperature, and the heat of formation.

Table 1: Parameters for Ti phases.

parameter	α	β	ω	liquid
ρ_{ref} (g/cc)	4.5018	4.5174	4.5810	-
ρ_0 (g/cc)	4.5405	4.5521[a]	4.6205	same as β
β_0 (GPa)	111.0	105.0[a]	115.0	same as β
β'_0	3.48	3.25[a]	3.35	same as β
RTFD	7.0	8.75	7.0	same as β
Γ_{ref}	1.184	1.010	1.184	-
Θ_{ref} (K)	368.0	317.0	368.0	-
$\Delta_f H^0$ (MJ/kg)	0.0	0.0859	0.0353	-
ECOH (MJ/kg)	-	-	-	9.8926
RLJ (g/cc)	-	-	-	4.05
FACLJ	-	-	-	1.0
EFAC (MJ/kg)	-	-	-	0.404
w_{liq}	-	-	-	1.08

[a] These values were used for pressures below 124 GPa. The values of Akahama, et al. [19], ρ_0 = 5.5995 g/cc, β_0 = 211.2 GPa, β'_0 = 3.24, were used at pressures above 145 GPa, as discussed in the text.

2.3 Fluid Phase

The thermodynamic functions for the fluid phase were computed using the CRIS model [13][38][39], along with the contributions from thermal electronic excitation. The CRIS model also uses a zero-Kelvin isotherm that is used to compute the potential energy of an atom in the cage formed by its neighbors. When several solid phases are present, as in this case, experience has shown that best results are usually obtained by using the highest-density phase. In this work, we have used the zero-Kelvin curve for the β phase, which is the most compressible phase at high pressures. The liquid model also requires five additional parameters.

- The zero-Kelvin curve must be extended into tension using the so-called LJ match option, requiring three parameters—ECOH, RLJ, and FACLJ. ECOH, the binding energy, was computed from the heat of formation data.

- The parameters EFAC and w_{liq} are used for "tuning" the model to match the enthalpy and entropy of the liquid at the melting point.

The energy zero for the liquid was set by using the same energy shift as for the α phase. Table 1 lists the parameters for the fluid phase.

2.4 Results

The model results are compared to zero-pressure thermophysical data and isobaric expansion measurements in Fig. 1. The agreement is satisfactory for the solid region and for the enthalpy and entropy of the liquid phase. The density of liquid Ti is not well known. Paradis and Rhim [41] list several measurements of the liquid density, including their own, from the melting point to 2400K. Our model prediction is within the envelope of these measurements, shown by triangles with error bars in Fig. 1. There are two sets of isobaric expansion measurements that give somewhat lower densities [42]. The discrepancies between these different sets of data are not yet understood.

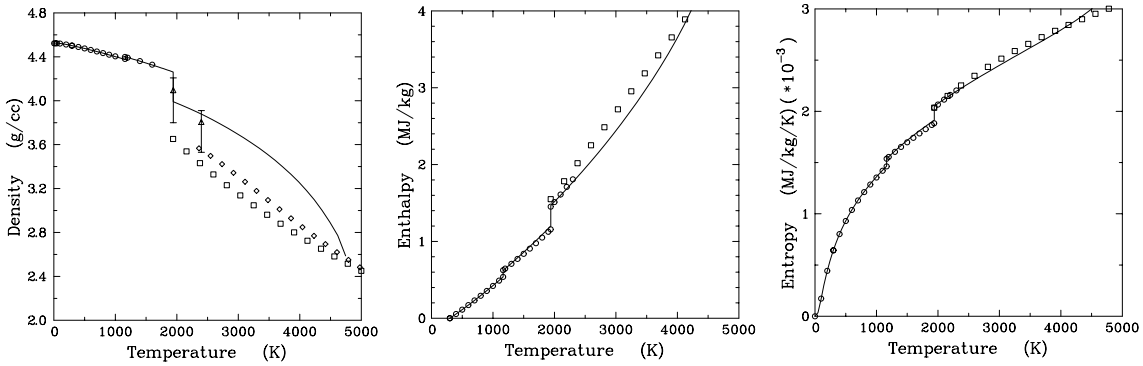

Fig. 1. Comparison of model with thermophysical data for Ti. Density: circles—solid at P=0 [28][29], triangles with error bars—liquid [41], squares and diamonds—isobaric expansion data for liquid at 0.3 GPa [42]. Enthalpy and entropy: circles—solid and liquid at P=0 [30], squares—isobaric data for liquid at 0.3 GPa [42]. Solid lines are from model.

Figure 2 compares the room-temperature isotherms for the three solid phases with experimental data and theoretical calculations. The α-phase curve agrees well with the experimental data of Vohra, et al. [31], which go up to 7 GPa, and the calculations of Ostanin and Trubitsin (OT) [24] at high pressures. The ω-phase curve also agrees with the low-pressure static data [31] and with the one data point of Xia, et al. [32], at 87 GPa. It is somewhat softer than OT and the data of Akahama, et al. [19]; however, a stiffer curve would not agree with the Hugoniot data and would give too low a pressure for the ω–β transition. The β-phase curve is in good agreement with OT up to 120 GPa. The data of Akahama, et al. [19], indicate a stiffening of the isotherm at high pressures, upon entering the δ-phase. The β curve was modified to match the high-pressure data, as explained above.

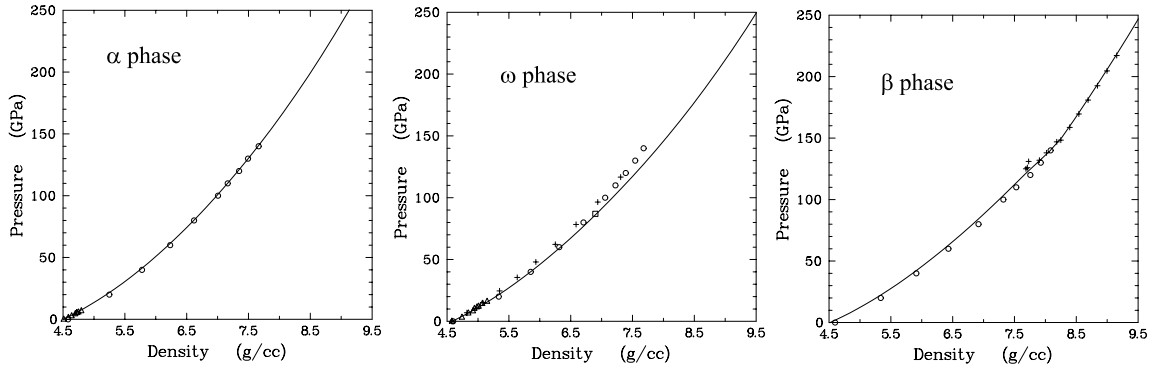

Fig. 2. Room temperature isotherms for Ti phases. Triangles—[31], crosses—[19], square—[32], circles—[24]. Solid lines are from model.

The titanium Hugoniot is shown in Fig. 3. The left side of the figure compares the calculated curve with experimental data up to about 300 GPa [34]-[36]. Strength terms were included in computing the Hugoniot in the solid region; the same parameters, taken from Steinberg [43], were used for all three solid phases. The strength corrections are significant; they stiffen the Hugoniot and also give rise to an elastic precursor with a velocity of 6.16 km / s. The phase transitions give rise to structure in the Hugoniot curve, as discussed below. The right side of Fig. 3 shows the Hugoniot in the ultra-high pressure region.

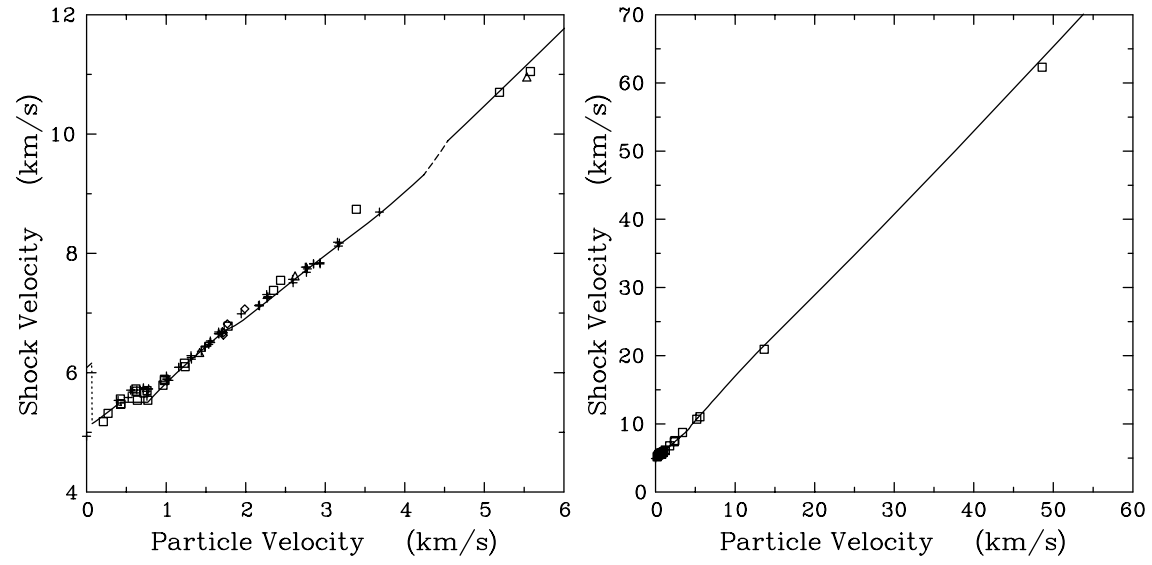

Fig. 3. Titanium Hugoniot in shock velocity-particle velocity plane. Curves were computed from model; dashed region shows melting, dotted region shows velocity drop behind elastic precursor. Left side gives data up to about 300 GPa, shown by crosses [33], squares [34][37], triangles [35], and diamonds [36]. Right side extends plot to ultra-high pressure of 14 TPa.

The predicted phase diagram and Hugoniot are shown in Fig. 4. The equilibrium α–ω transition pressure appears to be 7-8 GPa at room temperature [16][19]. We have deliberately chosen parameters that give a transition pressure of 10 GPa in order to match the shock wave measurements. The model predicts the onset of the α–ω phase transition at a stress of 10.7 GPa on the Hugoniot, in good agreement with the value 10.4 obtained by Gray, et al. [27]. This transition leads to the region of constant shock velocity at U_s=5.5 km/s, seen in Fig 3. There is considerable scatter in the Hugoniot data near the transition. The older shock data indicated a higher transition stress, 17.5 GPa; the discrepancy is thought to be due to the use of low-purity titanium samples [27].

As seen in Fig. 4, the α–β transition temperature decreases with pressure until it intersects the α–ω boundary, forming a triple point at 960K and 10.4 GPa. The ω–β transition temperature increases with pressure to 35 GPa, then decreases with increasing pressure. The ω–β phase boundary is very sensitive to the zero-Kelvin parameters for the two phases; a stiffer isotherm for the ω-phase would give too low a pressure for the ω–β transition at room temperature. The parameters used here predict the ω–β transition at 115 GPa, in reasonable agreement with the value 124 GPa obtained by Akahama, et al. [19].

The model predicts the ω–β transition to occur over the range 52-60 GPa on the Hugoniot. This transition gives rise to a slight softening in the Hugoniot at particle velocites in the range 1.75-1.95 km/s, as seen in the experimental data. The dotdash line in Fig. 4 is a release isentrope from the 86.5 GPa shock state of the solid, which intersects the zero pressure axis near the α–β transition pressure. This result agrees with the experiments of Kanel, et al. [44], who observed a drop in the surface reflectivity of titanium for shock pressures over the range 82.5 to 90.8 GPa.[1]

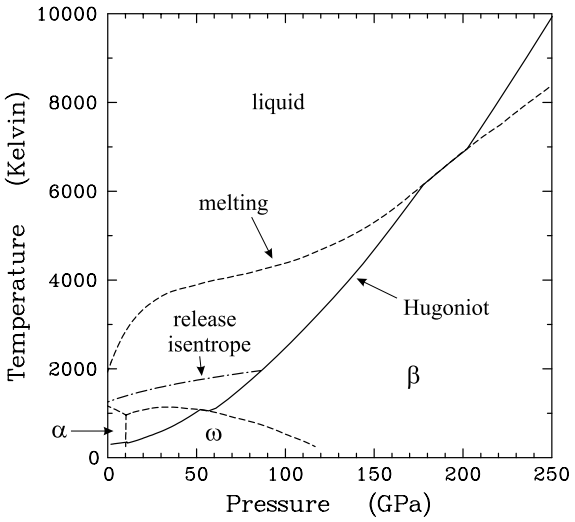

Fig. 4. Calculated phase diagram and Hugoniot for Ti. Phase boundaries are shown by dashed lines, the Hugoniot by a solid line. The dotdashed line is a release isentropre from a 86.5 GPa shock state.

The model predicts shock melting to begin at 178 GPa and be complete at 202 GPa. The dashed portion of the Hugoniot in Fig. 3 corresponds to the melting region. The model predicts an increase in shock velocity due to melting and also a small increase in the slope of the

1. Kanel, et. al., attributed the drop in reflectivity to melting but noted that the pressure was lower than expected for melting. We believe that the phenomenon is actually due to the α–β transition.

shock velocity-particle velocity curve. However, there are not enough experimental data to test this prediction. The onset of shock melting can be inferred experimentally by measuring the sound speed behind the shock front. Unfortunately, measurements of this type are not available for titanium.

It should be noted that the phase boundaries are quite sensitive to some of the model parameters. In particular, the onset of shock melting depends upon the density dependence of the Grüneisen function; a higher value of $\Gamma(\rho)$ would lower the melting temperature. New measurements of the Hugoniot and sound speed in this region would locate the ω–β and melting transitions more accurately.

Figure 5 compares the model predictions with Hugoniot data for porous titanium having initial densities ranging from 0.80-4.03 g/cc. These shock states cover a wide range of densities and temperatures. For example, the highest data point for an initial density of 1.80 g/cc corresponds to a shock state of 5.1 g/cc, 106 GPa, and 25,000K. The model is in good agreement with all of the data for porous titanium, showing that it is accurate at states far from the principal Hugoniot.

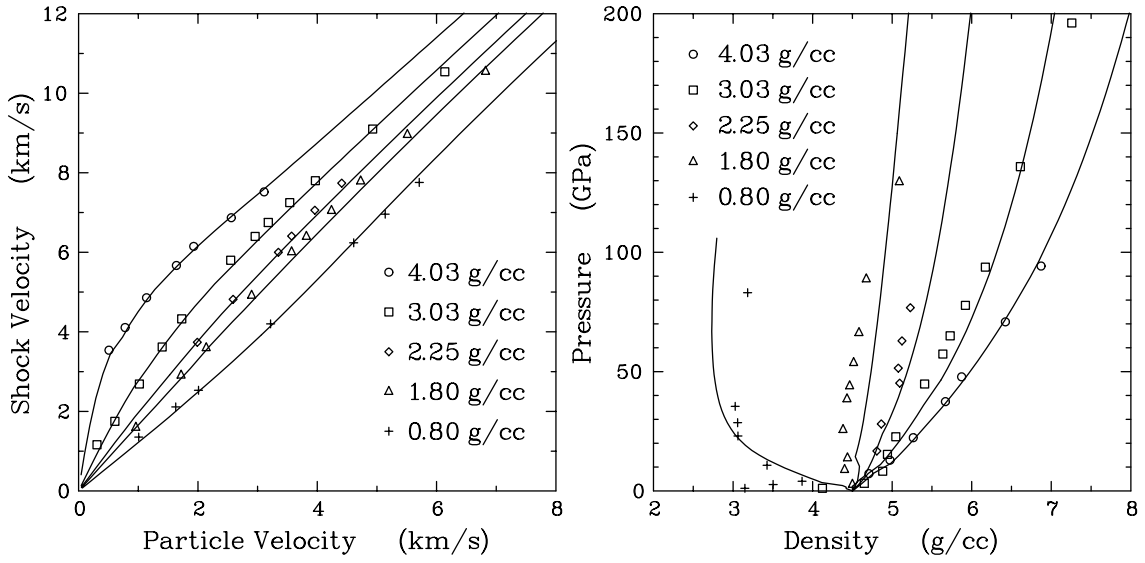

Fig. 5. Hugoniot for porous titanium. Experimental data are from Ref. [34].

In constructing the EOS table, special attention was given to the treatment of tension and vaporization. Maxwell constructions were included at temperatures above the boiling point, so that the EOS describes equilibrium vaporization at high temperatures. A nonequilibrium tensile region was left at temperatures below the boiling point, so that the EOS will give a correct prediction of spallation in hydrodynamic code calculations.

The behavior of the EOS in the vapor-liquid region is shown in Fig. 6. The pressure is plotted as a function of density on 25 isotherms from 3700K to 25,000K. The EOS exhibits a "plasma phase transition" (PPT) at temperatures above 4690K and below 5800K, at densities in the range 1.7-2.7 g/cc. This feature, which was also predicted in our models for aluminum [10], nickel [13], and copper [14], arises from the effect of the metal-insulator transition on the thermal electronic contribution to the EOS. At temperatures below 4690K, there is a single coexistence region between the vapor and the metallic liquid. At higher temperatures, there are two coexistence regions, one between the vapor and an insulating liquid, the other from the insulating liquid to the metallic liquid. The predicted critical point (for the vapor and the insulating liquid) is at 15,500K, 0.7 GPa, and 0.5 g/cc. The existence of a PPT has not yet been demonstrated in any metal, and this region of the EOS surface requires further study.

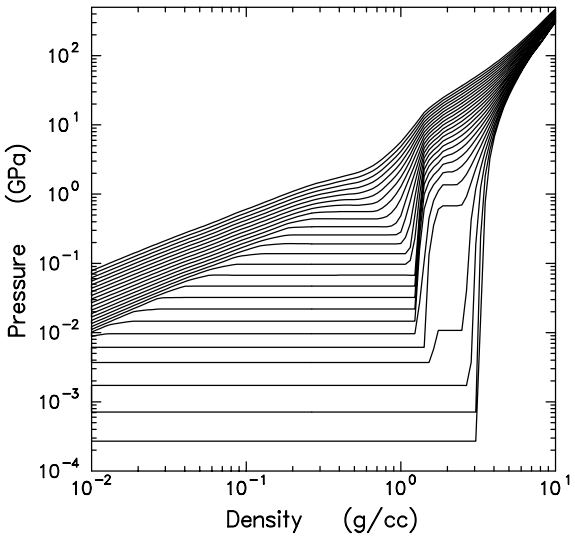

Fig. 6. EOS of titanium in vapor-liquid transition region. There are 25 isotherms at temperatures from 3700K to 25,000K, equally spaced in the logarithm.

The EOS table for titanium covers the density range from 0.0 to 400 g/cc and the temperature range from 5 to 1.0×10^{8} K. It has been given material number 2970.

3. Ti6Al4V Alloy

3.1 General

The alloy Ti6Al4V has the nominal composition 90% Ti / 6% Al / 4% V by weight. The corresponding atomic composition is 86.2% Ti / 10.2% Al / 3.6% V. The average atomic weight is 45.859, compared with 47.88 for pure Ti. Actual samples vary from the nominal composition. For example, the material studied by Gray, et al. [27], was 89.06% Ti / 6.33% Al / 4.23% V / 0.38%, with 0.38% other elements.

Little is known about the phase diagram of the alloy. We will rely heavily on our model for pure titanium, together with some theoretical considerations, to construct an EOS that matches the available data. In particular, the model must be consistent with the following information.

- The shock velocity-particle velocity curve for Ti6Al4V agrees fairly well with that for pure Ti at low pressures but is much stiffer above 10 GPa.
- Unlike pure Ti, Ti6Al4V does not transform to the ω-phase at shock pressures up to 25 GPa [27].
- The Hugoniot for Ti6Al4V does show evidence of a phase transition near 40 GPa [45]. However, the Hugoniot above the transition is still stiffer than for pure Ti.

In this work, we will show that good agreement with all of the available data can be obtained with a model similar to that for pure Ti, but with two modifications. First, we eliminate the ω phase, leaving only the α, β, and fluid phases. Second, additive-volume mixing is used to determine the model parameters, resulting in the increased stiffness that is observed experimentally.

Before proceeding, we note that the Ti6Al4V is not pure α at RTP but contains a small amount of the β-phase [27]. We will not attempt to deal with this complication explicitly and will continue to refer to the ambient phase as "α."

3.2 Model Parameters

Our EOS models for the α, β, and fluid phases are identical to those for pure Ti, except for the model parameters. The EOS for the solid phases use the Birch-Murnaghan formula for the zero-Kelvin isotherm and the Debye model for the lattice vibrations. The EOS for the fluid phase uses the CRIS model and the same zero-Kelvin isotherm as the β phase. Thermal electronic contributions are also included in the EOS for the solid and fluid phases.

The amounts of Al and V in this alloy are not sufficient to cause the formation of Ti-Al or Ti-V compounds [46]; the alloy may be regarded as a mixture of elements.

Therefore, the additive-volume mixture approximation, though not exact for an alloy, is a reasonable starting point for the development of a model.

Figure 7 shows room temperature isotherms for the α and β phases, calculated from the additive-volume model. These calculations were made using the MOD MIX option in PANDA, using our tabular EOS for the titanium phases, the aluminum EOS discussed in Ref. [10], and a simple vanadium EOS table constructed specifically for use in this work.[1] The compressibility of the α phase is close to that for pure Ti up to 50 GPa. However, the isotherm for the β phase is considerably stiffer than that for pure Ti at high pressures, enough to explain the increased stiffness of the Hugoniot. The additive-volume calculation also gives a reasonable density for the α phase—4.372 g/cc, only 1% less than the experimental value, 4.418 g/cc. This result lends further credence to our use of this approximation.

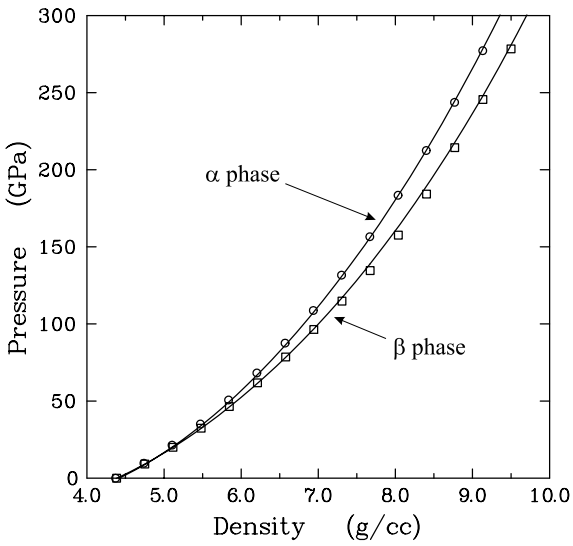

Fig. 7. Room temperature isotherms for Ti6Al4V. Circles (α phase) and squares (β phase) were computed by additive volume approximation. Solid lines are the fits.

In principle, additive-volume mixing could be used to construct the new EOS tables for all three phases. However, that procedure would require additional work on the EOS for both Al and V. Therefore, a simpler approach was adopted. Debye temperatures and Grüneisen parameters for the two solid phases were estimated by averaging the values for the pure elements, weighted by their mass fractions. The zero-Kelvin parameters were then chosen to fit the results of the additive-volume calculations. The fits are compared to the additive-volume calculations in Fig. 7. (The fit for the α phase was chosen to match the experimental RTP density instead of the calculated value.) The heat of formation $\Delta_f H^0$ for the β phase was taken from that for pure Ti, multiplied by the mass fraction of Ti.

For the liquid phase, the cohesive energy was computed by summing the cohesive energies for the three elements, weighted by their mass fractions. The other parameters were kept the same as for pure Ti.

The parameters for all three phases of the alloy are given in Table 2.

1. The vanadium EOS was constructed using the same model discussed in Sec. 16.1 and Appendix E of the PANDA manual. Only the solid phase was used in these calculations.

Table 2: Parameters for Ti6Al4V phases.

parameter	α	β	liquid
ρ_{ref} (g/cc)	4.4180	4.3856	-
ρ_0 (g/cc)	4.4588	4.4233	same as β
β_0 (GPa)	111.0	103.0	same as β
β'_0	3.58	3.35	same as β
RTFD	7.0	6.0	same as β
Γ_{ref}	1.250	1.100	-
Θ_{ref} (K)	371.0	326.0	-
$\Delta_f H^0$ (MJ/kg)	0.0	0.0773	-
ECOH (MJ/kg)	-	-	10.0
RLJ (g/cc)	-	-	3.90
FACLJ	-	-	1.0
EFAC (MJ/kg)	-	-	0.404
w_{liq}	-	-	1.08

A special thermal electronic table was also constructed for the alloy, using the electronic tables for pure Ti and Al. Because we do not have a thermal electronic table for V, the mixture was taken to have an atomic composition 89.8% Ti / 10.2% Al. (V is adjacent to Ti in the periodic chart, so this approximation should give satisfactory results.) The entropies of the two components were added together, weighted by their atomic fractions, at constant atomic volumes.

3.3 Results

Figure 8 shows the Hugoniot for Ti6Al4V in the shock velocity-particle velocity plane. Figure 9 shows the phase diagram and Hugoniot in the pressure-temperature plane. The model predictions agree very well with the experimental Hugoniot data [36][45][47]-[49], including several features associated with phase transitions. Steinberg's parameters for the alloy [43] were used to include strength terms in the solid region. The strength corrections are significant, just as they were in pure Ti; they stiffen the Hugoniot slightly and give rise to an elastic precursor with a velocity of 6.21 km / s.

The model predicts the α–β transition to occur at 56 GPa at room temperature. Under shock loading, it occurs at a stress of 42 GPa, with a 4% volume change, in good agreement with the Hugoniot data [45].

The model predicts shock melting to begin at 182 GPa and be complete at 207 GPa, almost the same as in pure Ti. The dashed portion of the Hugoniot in Fig. 8 corresponds to the melting region. As in pure Ti, there is an increase in shock velocity due to melting. This prediction agrees with the anomalous behavior seen in the data. The data points of Winfree, et al. [47], shown by squares in Fig. 8, do not lie on an extrapolation of the lower pressure data. Their data show a marked stiffening of the Hugoniot over the highest density point of Hixon [49], shown by circles in Fig. 8. Taking the two sets of data together, there is a striking 6.5% increase in the shock velocity with only 5.6% increase in the particle velocity. The model shows that this unusual behavior arises from melting.

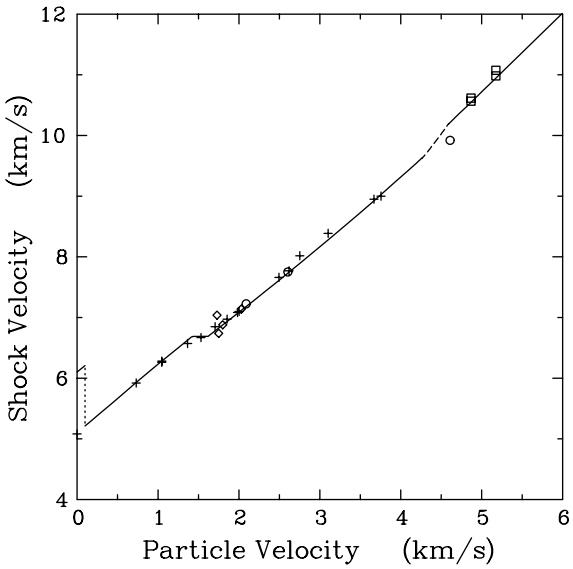

Fig. 8. Ti6Al4V Hugoniot in shock velocity-particle velocity plane. Curves were computed from model; dashed region shows melting, dotted region shows velocity drop behind elastic precursor. Data: crosses [45][48], circles [49], squares [47], and triangles [36].

Hixon's data point shows that the model underestimates the onset of shock melting by about 20 GPa (10%). This discrepancy could easily be corrected by small changes in the model parameters, particularly the Grüneisen parameter for the β phase. However, we have not made that adjustment in the present work, preferring to wait until additional experimental data become available in this regime.

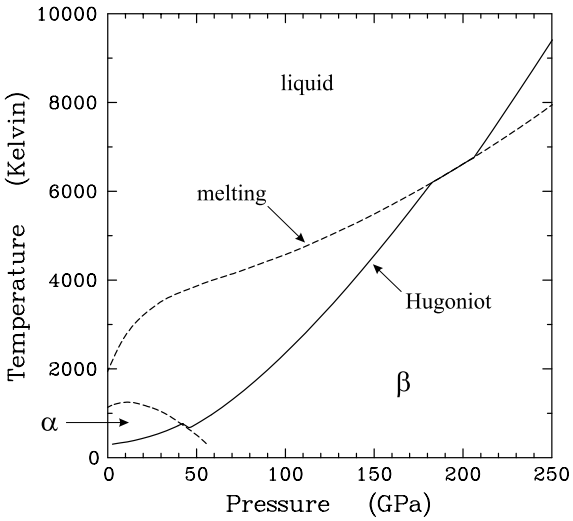

Fig. 9. Calculated phase diagram and Hugoniot for Ti6Al4V. Phase boundaries are shown by dashed lines, the Hugoniot by a solid line.

As for pure Ti, the EOS table for the alloy includes Maxwell constructions for temperatures above the boiling point, leaving a nonequilibrium tensile region at low temperatures. The EOS table covers the density range from 0.0 to 400 g/cc and the temperature range

from 5 to 1.0×10^8 K. It has been given material number 4061. The behavior of the EOS in the vapor-liquid region is similar to that for pure titanium, shown in Fig. 6, including the PPT.

Chhabildas has obtained time-dependent data on Ti6Al4V shocked to 220 GPa [50]. The same technique used in Ref. [47] was used to accelerate a flyer plate to a velocity of 9.6 km/s, which then impacted a target plate backed by a LiF window. The particle velocity at the target-window interface was measured using the VISAR method. The flyer and target, both Ti6Al4V, were 0.56 and 2.0 mm in thickness, respectively. Figure 10 compares a CTH calculation of this experiment, using our new EOS table, with the experimental data. (The data have been shifted in time to match the calculation, since the arrival time was not determined in the experiment.) The flyer plate is heated during acceleration, and an initial temperature of 600K was assumed in the calculation. The calculation gives an initial shock pressure of 220 GPa in the flyer and target. This state is close to the lower Hugoniot point from Ref. [47], shown by squares in Fig. 8. Hence it lies in the liquid region. The rarefaction from the rear surface of the flyer overtakes the shock front just as it impacts the window. Impact with the window simultaneously drops the shock pressure to 180 GPa. The calculation is in good agreement with the experimental data.

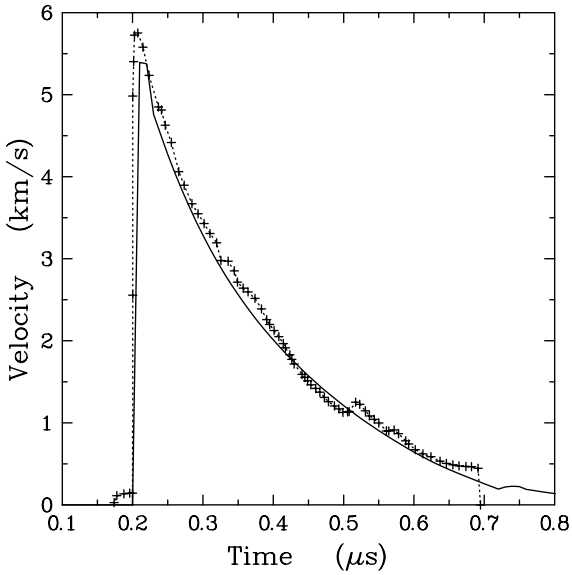

Fig. 10. Interface particle velocity for shock-release experiment on Ti6Al4V. Experimental data [50] are shown by crosses connected by a dotted line. CTH calculation is shown by a solid line.

4. Conclusions and Recommendations

The present report describes new EOS tables for titanium (material number 2970) and the alloy Ti6Al4V (material number 4061). These tables are significantly better than those currently available in the CTH database [8][9]. They should be added to file “sesame” and set as the default materials in the CTH file EOS_data [5][6].

Experience has shown that no EOS modeling effort is ever fully finished—further refinements are always possible and desirable. In this case, the following tasks are particularly worthy of consideration.

- Further investigation of shock melting is needed for both pure Ti and the alloy. The EOS model predicts an unusually large increase in shock velocity near 200 GPa, due to melting. This prediction agrees with three recent Hugoniot data points for Ti6Al4V. However, more measurements are needed to confirm these findings. An accurate EOS for Ti6Al4V is especially important for impedance matching calculations in the SNL three-stage gun experiments. Measurements of the sound speed in this region would also be very useful. Some revision of the EOS may be needed when new data become available.

- The model predicts a plasma phase transition in the vapor-liquid critical region for both Ti and Ti6Al4V. Further theoretical and experimental work is needed to determine if such a transition actually exists and what effect it could have on the material behavior.

References

[2] J. M. McGlaun, F. J. Ziegler, S. L. Thompson, L. N. Kmetyk, and M. G. Elrick, “CTH - User's Manual and Input Instructions,” Sandia National Laboratories report SAND88-0523, April 1988.

[3] J. M. McGlaun, S. L. Thompson, and M. G. Elrick, “CTH: A Three-Dimensional Shock Wave Physics Code,” Int. J. Impact Engng. 10, 351-360 (1990).

[4] J. M. McGlaun, S. L. Thompson, L. N. Kmetyk, and M. G. Elrick, “A Brief Description of the Three-Dimensional Shock Wave Physics Code CTH,” Sandia National Laboratories report SAND89-0607, July 1990.

[5] E. S. Hertel, Jr. and G. I. Kerley, “CTH EOS Package: Introductory Tutorial,” Sandia National Laboratories report SAND98-0945, 1998.

[6] E. S. Hertel, Jr. and G. I. Kerley, “CTH Reference Manual: The Equation of State Package,” Sandia National Laboratories report SAND98-0947, 1998.

[7] G. I. Kerley, “CTH Equation of State Database: MGRUN Option,” Kerley Publishing Services report KPS00-4, June 2000.

[8] The status of existing EOS models is discussed in several on-line documents in the CTH /data subdirectory. The default EOS tables are discussed in file tables.ref.

[9] G. I. Kerley, “Progress on CTH EOS Database,” memorandum to P. A. Taylor and E. S. Hertel, Jr., June 15, 2000.

[10] G. I. Kerley, “Theoretical Equation of State for Aluminum,” Int. J. Impact Engng. **5**, 441-449 (1987).

[11] G. I. Kerley, “Multiphase Equation of State for Iron,” Sandia National Laboratories report SAND93-0027, 1993.

[12] G. I. Kerley and L. C. Chhabildas, “Multicomponent-Multiphase Equation of State for Carbon,” Sandia National Laboratories report SAND2001-2619, 2001.

[13] G. I. Kerley, “Equations of State for Be, Ni, W, and Au,” Sandia National Laboratories report SAND2003-3784, October 2003.

[14] G. I. Kerley, “Equations of State for Copper and Lead,” Kerley Technical Services report KTS02-1, February 2002.

[15] G. I. Kerley, “User’s Manual for PANDA II: A Computer Code for Calculating Equations of State,” Sandia National Laboratories report SAND88-2291, 1991.

[16] J. F. Cannon, ‘‘Behavior of the Elements at High Pressures,’’ J. Phys. Chem. Ref. Data 3, 781-824 (1974).

[17] D. A. Young, ‘‘Phase Diagrams of the Elements,’’ Lawrence Livermore Laboratory report UCRL-51902, September 11, 1975.

[18] Y. K. Vohra and P. T. Spencer, “Novel γ-Phase of Titanium at Megabar Pressures,” Phys.Rev. Lett. 86, 3068-3071 (2001).

[19] Y. Akahama, H. Kawamura, and T. Le Bihan, “New δ (Distorted-bcc) Titanium to 220 GPa,” Phys.Rev. Lett. 87, 275503-1 (2001).

[20] J. C. Jamieson, “Crystal Structures of Titanium, Zirconium, and Hafnium at High Pressures,” Science 18, 72-72 (1963).

[21] H. Xia, S. J. Duclos, A. L. Ruoff, and Y. K. Vohra, “New High Pressure Phase Transition in Zirconium Metal,” Phys. Rev. Lett. 64, 204-207 (1990).

[22] H. Xia, G. Parthasarathy, H. Luo, Y. K. Vohra, and A. L. Ruoff, “Crystal Structures of Group IVa Metals at Ultrahigh Pressures,” Phys. Rev. B 42, 6736-6738 (1990).

[23] R. Ahuja, J. M. Wills, B. Johansson, and O. Eriksson, “Crystal Structures of Ti, Zr, and Hf Under Compression: Theory,” Phys. Rev. B 48, 16269-16279 (1993).

[24] S. A. Ostanin and V. Yu. Trubitsin, “A simple model for calculating the P-T phase diagram of Ti,” J. Phys.: Condens. Matter 9, L491-L496 (1997).

[25] A. R. Kutsar, V. N. German, and G. I. Nosova, “(α->ω Transition in Titanium and Zirconium in Shock Waves,” Sov. Phys. Dokl. 18, 733-734 (1973).

[26] A. R. Kutsar, M. N. Pavlovskii, and V. V. Komissarov, “Observation of a Two-Wave Shock Configuration in Titanium,” JETP Lett. 35, 108-112 (1982).

[27] G. T. Gray III, C. E. Morris, and A. C. Lawson, “Omega Phase Formation in Titanium and Titanium Alloys,” in Titanium ‘92 Science and Technology, edited by F. H. Froes and I. Caplan (The Minerals, Metals & Materials Society, 1993).

[28] Handbook of Chemistry and Physics, edited by David R. Lide (CRC Press, Boca Raton, 1996) 77^{th} edition.

[29] Y. S. Touloukian, R. K. Kirby, R. E. Taylor, and T. Y. R. Lee, ‘‘Thermal Expansion, Nonmetallic Solids,’’ Thermophysical Properties of Matter (IFI/Plenum, New York, 1977) Vol. 13.

[30] M. W. Chase, Jr., C. A. Davies, J. R. Downey, Jr., D. J. Frurip, R. A. McDonald, and A. N. Syverud, “JANAF Thermochemical Tables,” J. Phys. Chem. Ref. Data 14, Supp. No. 1 (1985).

[31] Y. K. Vohra, H. Olijnyk, W. Grosshans, and W. B. Holzapfel, “Equation of State Measurements of α, β, and ω-Ti by High Pressure Energy Dispersive X-ray Diffraction,” in Proc. 8th AIRAPT Conf. High Pressure in Research and Industry (Uppsala) 1981, pp. 354-357.

[32] H. Xia, G. Parthasarathy, H. Luo, Y. K. Vohra, and A. L. Ruoff, “Crystal Structures of Group IVa Metals at Ultrahigh Pressures,” Phys. Rev. B 42, 6736-6738 (1990).

[33] S. P. Marsh, LASL Shock Hugoniot Data (University of California, Berkeley, 1980).

[34] R. F. Trunin, G. V. Simakov, and A. B. Medevdev, “Compression of Titanium in Shock Waves,” High Temp. 37, 851-856 (1999).

[35] W. M. Isbell, F. H. Shipman, and A. H. Jones, “Hugoniot Equation of State of Eleven Materials to Five Mbars,” Materials Science Laboratory report MSL-68-13.

[36] P. Andriot, P. Lalle, and J. P. Dejean, “Elastic Behavior of Pure Titanium and TA6V4 Titanium Alloy at High Pressure,” in High Pressure Science and Technology - 1993, edited by S. C. Schmidt, J. W; Shaner, G. A. Samara, and M. Ross (AIP Conference Proceedings 309, 1994) pp. 1009-1012.

[37] R. F. Trunin, L. A. Il’kaeva, M. A. Podurets, L. V. Popov, B. V. Pechenkin, L. V. Prokhorov, A. G. Sevast’yanov, V. V. Khrustalev, “Shock compressibility Measurements for Iron, Copper, Lead, and Titanium Under Pressures of 20 TPa,” High Temp. 32, 646-649 (1994).

[38] G. I. Kerley, “Perturbation Theory and the Thermodynamic Properties of Fluids II. The CRIS Model,” J. Chem. Phys. 73, 478-486 (1980).

[39] G. I. Kerley, “A Model for the Calculation of Thermodynamic Properties of a Fluid Using Hard-Sphere Perturbation Theory and the Zero-Kelvin Isotherm of the Solid,” in Molecular Based Study of Fluids, edited by J. M. Haile and G. A. Mansoori (Am. Chem. Soc., Washington, DC., 1983) pp 107-138.

[40] D. A. Liberman, “Self-Consistent Field Model for Condensed Matter,” Phys. Rev. B 20, 4981-4989 (1979).

[41] P.-F. Paradis and W.-K. Rhim, "Non-Contact Measurements of Thermophysical Properties of Titanium at High Temperatures," J. Chem. Thermo. 32, 123-133 (2000).

[42] G. R. Gathers, "Dynamic Methods for Investigating Thermophysical Properties of Matter at Very High Temperatures and Pressures," Rep. Prog. Phys. 49, 341-396 (1986). Two sets of data are given for titanium. Data from table 13 (Kiel) is shown by squares in Fig. 1. Table 32 (Livermore) gives only density vs. enthalpy; these densities are higher than those of table 13. A curve of density vs. temperature, obtained by using the density from table 32 and the enthalpy from table 13, is shown by diamonds in Fig. 1.

[43] D. J. Steinberg, "Equation of State and Strength Properties of Selected Materials," Lawrence Livermore National Laboratory report UCRL-MA-106439, 1991.

[44] G. I. Kanel, K. Baumung, D. Rush, J. Singer, S. V. Razorenov, and A. V. Utkin, "Melting of Shock-Compressed Metals in Release," in Shock Compression of Condensed Matter - 1997, edited by S. C. Schmidt, D. P. Dandekar, and J. W. Forbes (AIP Conference Proceedings 429, 1998) pp. 155-158.

[45] C. E. Morris, M. A. Winkler, and A. C. Mitchell, "Ti-6%Al-4%V Alloy Wave Profile Measurements in the Shadow Region," in Shock Waves in Condensed Matter - 1987, edited by S. C. Schmidt and N. C. Holmes (North-Holland, Amsterdam, 1988) pp. 155-158.

[46] F. H. Hayes, "The Al-Ti-V (Aluminum-Titanium-Vanadium) System," J. Phase Equil. 16, 163-176 (1995).

[47] N. A. Winfree, L. C. Chhabildas, W. D. Reinhart, D. E. Carroll, and G. I. Kerley, "EOS Data of Ti-6Al-4V to Impact Velocities of 10.4 km/s on a Three-Stage Gun," presented at the 2001 APS Meeting on Shock Compression of Condensed Matter, in press.

[48] Data of C. E. Morris, Los Alamos National Laboratory, cited in Ref. [47].

[49] Data of R. Hixson, Los Alamos National Laboratory, cited in Ref. [47].

[50] L. C. Chhabildas, "Hypervelocity Impact Phenomena," in Metall. Mater. Appl. Shock-Wave High-Strain-Rate Phenom., edited by L. E. Murr, K. P. Staudhammer, and M. A. Meyers (Elsevier, Amsterdam, 1995), pp. 245-256.

Appendix A

Plots of Tension Region

The following plots have been included in response to a request for more information about the tension region of the tables. All EOS models that have a realistic treatment of the vapor-liquid transition display van der Waals loops at low temperatures. The equilibrium vapor-liquid transition is described by the "Maxwell construction." At a given temperature, the two-phase region is defined by the densities at which the vapor and liquid have equal pressures and Gibbs free energies. The pressure is constant in the two-phase region, while the energy is given by a volume-weighted average.

In generating an EOS table, we normally include the Maxwell constructions at temperatures above the boiling point but allow a tension region at low temperatures so that the EOS can be used in hydrocode calculations that treat spallation behavior. Unfortunately, the inconsistency inherent in this procedure leads to negative heat capacities and other numerical problems at densities below the liquid spinodals. PANDA eliminates this problem by substituting well-behaved functions at low temperatures and densities. (See Sec. 13.5 of the PANDA manual [15].)

The resulting tension regions for Ti and Ti6Al4V are shown in Fig. 11. Since tensile strengths for these materials are typically 2.5-5.0 GPa, the tables should give a reasonable description of spallation behavior in most cases. In unusual cases, i.e., where a material is very hot when it goes into tension, it may be necessary to use a temperature-dependent fracture model or simply reduce the fracture strength to avoid getting into the artificial region.

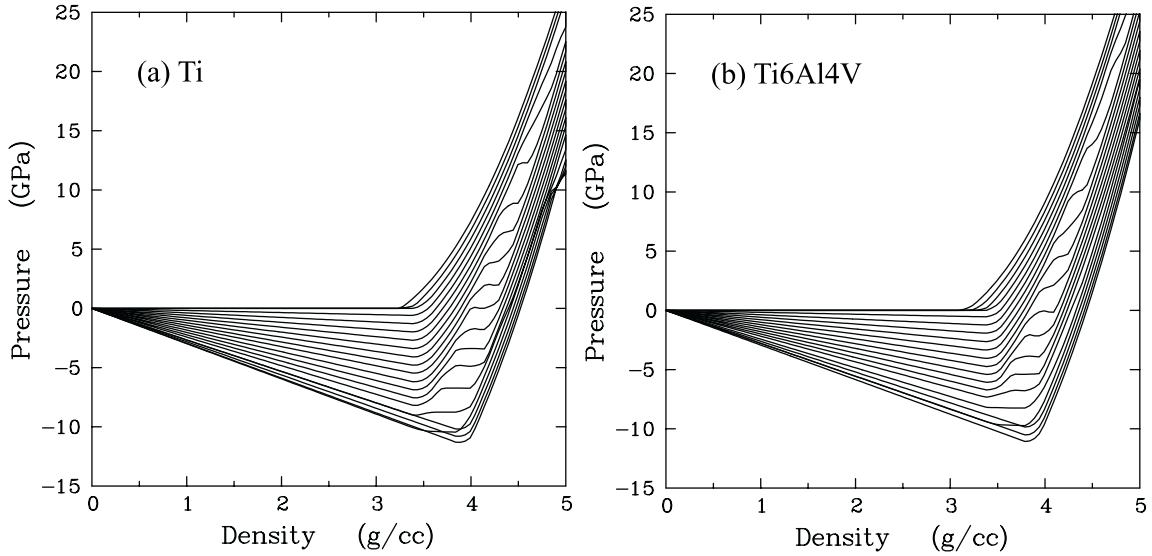

Fig. 11. Plots of tension region for Ti and Ti6Al4V. There are 20 isotherms from 100 to 4000K, equally spaced in temperature.

Distribution

1 Alliant TechSystems
Attn: Frederick Stecher
MS: MN07-MW44
4700 Nathan Lane N.
Plymouth, MN 55442-2512

3 Applied Research Associates, Inc.
Attn: Dennis Grady
Craig Doolittle
K. Bryan Milligan
4300 San Mateo Blvd. NE, Suite A-220
Albuquerque, NM 87110

1 Applied Research Associates, Inc.
Attn: William Brown
2760 Eisenhower Ave., Suite 308
Alexandria, VA 22314

1 Applied Research Associates
Attn: Peter Dzwilewski
5941 South Middlefield Rd., Suite 100
Littleton, CO 80123

2 Battelle Memorial Institute
Attn: Dale Trott
Mike Fisher
505 King Ave.
Columbus, OH 43201-2693

1 Boeing Corporation
Attn: Kevin Housen
MS 2T-50
P. O. Box 3999
Seattle, WA 98124

1 Boeing Company
Attn: Irene Aronoff
MC QB-62
PO Box 7922
Canoga Park, CA 91309-7922

1 Brown University
Attn: Peter Schultz
Dept. of Geological Sciences
P.O. Box 1846
Providence, RI 02912

1 Brigham Young University
Attn: Carl Sorenson
Dept. of Mech. Engineering
Provo, UT 84602

1 California Institute of Technology
Attn: Thomas Ahrens
Seismological Laboratory
1299 E. California Blvd.
Pasadena, CA 91125

1 California Institute of Technology
Attn: Joseph Shepherd
Engineering and Applied Science
MC 105-50
Pasadena, CA 91125

3 Carnegie Institution of Washington
Geophysical Laboratory
Attn: T. S. Duffy
R. M. Hemley
H. K. Mao
5251 Broad Branch Rd., NW
Washington, DC 20015

1 Cornell University
Department of Physics
Attn: Neil W. Ashcroft
Ithaca, NY 14853

1 Cornell University
Materials Science & Engineering
Attn: Arthur L. Ruoff
Ithaca, NY 14853

1 Enig Associates, Inc.
Attn: Julius W. Enig
11120 New Hampshire Ave., Suite 500
Silver Spring, MD 20904-26

1 Harvard University
Attn: Sarah Stewart-Mukhopadhyay
Department of Earth & Planetary Sciences
Cambridge, MA 02138

1 Institute for Defense Analyses
Attn: Bohdan Balko
1801 North Beauregard Street
Alexandria, VA 22311

15 Kerley Technical Services
Attn: Gerald I. Kerley, Consultant
P.O. Box 709
Appomattox, VA 24522-0709

1 KTech
Attn: Larry Lee
2201 Buena Vista SE, Suite 400A
Albuquerque, NM 87106-4265

2 Lockheed Martin Missiles Space Systems
Missiles & Space Operations
Attn: Erik Matheson
Luen Tam
1111 Lockheed Martin Way
Sunnyvale, CA 94089

2 NASA Johnson Space Center
Attn: Eric L. Christiansen
Justin H. Kerr
Mail Code SN3
Houston, TX 77058

2 NASA/Langley Research Center
Attn: Scott A. Hill, MS 431
Carl Poteet, MS 396
1 North Dryden St.
Hampton, VA 23681-2199

5 Naval Air Warfare Center
Attn: Joseph B. Bickley
Thomas J. Gill
John Kandell
Kelly Minnick
Edwin Szymanski
1 Administrative Circle
China Lake, CA 93555

1 Naval Postgraduate School
ELectrical & Computer Engineering Dept.
Attn: Donald Wadsworth
833 Dyer Road, Bldg. 232
Monterey, CA 93943-5121

7 Naval Surface Warfare Center
Dahlgren Division
Attn: J. R. Cogar
R. Gamache
R. K. Garrett, Jr.
M. Hobson
D. F. Robinson
D. Vavrick
L. T. Wilson
17320 Dahlgren Rd.
Dahlgren, VA 22448

6 Naval Surface Warfare Center
Indian Head Division
Attn: Bill Lawrence
Phil Miller
Thomas P. Russell
Gerrit Sutherland
Daniel Tam
Frank J. Zerilli
101 Strauss Avenue
Indian Head, MD 20640-5035

2 Network Computing Services, Inc.
AHPCRC
Attn: Gordon R. Johnson
Tim Holmquist
1200 Washington Avenue South
Minneapolis, MN 55415

1 New Mexico State Inst. of Mining & Tech.
Attn: Robert Abernathy
EMRTC Center
Socorro, NM 87801

1 Oak Ridge National Laboratory
Attn: Seokho Kim
P. O. Box 2009
Oak Ridge, TN 37831-8045

1 Plattsburgh State University
Department of Physics
Attn: Paul P. Szydlik
101 Broad Street
Plattsburg, NY 12901-2681

1 Schlumberger Reservoir Completions
Center, Perforating Gun Systems
Attn: Wenbo Yang
14910 Airline Road
Rosharon, TX 77583

1 Science Applications International Corp.
Attn: Gerry Gurtman
10260 Campus Point Drive
San Diego, CA 92121

1 Science Applications International Corp.
Attn: Mark E. Beyers
1710 SAIC Drive
McLean, VA 22102

2 Southwest Research Institute
Attn: Charles E.Anderson
James Walker
P. O. Drawer 28510
San Antonio, TX 78228-0510

1 Texas A&M University
Nuclear Engineering Dept.
Attn: Bruce L. Freeman
Zachry Building, Room 129
College Station, Texas 77843-3133

1 Texas Tech University
Department of Mechanical Engineering
Attn: Darryl James
Box 41021
Lubbock, TX 79409-1021

2 Thiokol Corporation
Science & Engineering Division
Attn: Robert L. Hatch, Mailstop 244
Dwight Clark, Mailstop 280
P. O. Box 707
Brigham City, Utah 84302-0707

1 University of Alabama in Huntsville
Aerophysics Department
Attn: Mark Zweiner
P.O. Box 999
Huntsville, AL 35899

2 University of Arizona
Department of Planetary Sciences
Attn: W. B. Hubbard
H. J. Melosh
Tucson, AZ 85721

1 University of California
Attn: Raymond Jeanloz
Earth and Planetary Science
Berkeley, CA 94720-4767

15 University of California
Lawrence Livermore National Laboratory
Attn: R. Cauble
G. W. Collins
H. C. Graboske
J. Heidrich
N. C. Holmes
B. Militzer
B. Moran
J. A. Moriarty
A. K. McMahan
W. J. Nellis
P. C. Souers
C. M. Tarver
S. T. Weir
D. A. Young
G. B. Zimmerman
P.O. Box 808
Livermore, CA 94550

18 University of California
Los Alamos National Laboratory
Attn: Chris Adams
J. Boettger
L. A. Collins
L. L. Davis
R. Gustavsen
R. S. Hixson
B. L. Holian
Y. Horie
J. D. Johnson
J. E. Kennedy
J. D. Kress
J. Mace
E. S. Martin
R. Parker
J. M. Pedicini
J. P. Ritchie
S. Sheffield
D. Saumon
P.O. Box 1663
Los Alamos, NM 87545

1 University of Illinois
Attn: David M. Ceperley
Department of Physics
1110 W. Green Street
Urbana, IL 61801

1 University of Missouri-Rolla
CE Department
Attn: William Schonberg
Rolla, MO 65409

1 University of Notre Dame
Dept. of Aerospace and Mech. Eng.
Attn: Joseph M. Powers
372 Fitzpatrick Hall of Engineering
Notre Dame, Indiana 46556-5637

1 University of Rochester
Laboratory for Laser Energetics
Attn: R. L. McCrory
250 East River Road
Rochester, NY 14623-1299

1 University of Rochester
Physics & Astronomy
Attn: Hugh M. Van Horn
RC Box 270171
Rochester, NY 14627-0171

2 The University of Texas at Austin
Institute for Advanced Technology
Attn: Stephan J. Bless
David Littlefield
4030 W. Braker Lane, Suite 200
Austin, TX 78712

1 University of Texas at El Paso
Mechanical & Industrial Engineering
Attn: Michael Huerta
500 West University Avenue
El Paso, TX 79968

1 University of Washington
Dept. of Aeronautics and Astronautics
Attn: Keith A. Holsapple, FS10
Seattle, WA 98195

1 U.S. Air Force Inst. of Technology/ENY
Attn: Jay R. Anderson
Wright-Patterson AFB, OH 45433

1 U.S. Air Force Research Laboratory
Attn: David F. Medina
3550 Aberdeen Ave SE
Kirtland AFB, NM 87117-5776

10 U.S. Army Research Laboratory
Attn: W. Bruchey
D. Dandekar
F. Gregory
A. D. Gupta
Y. Huang
K. D. Kimsey
H. Meyer, Jr.
M. L. Normandia
S. Schoenfeld
J. Starkenberg
P.O. Box 334, Main Station
Aberdeen Proving Ground, MD 21005

3 U.S. Army Space & Missile Defense Command
Attn: Robert Becker
Jason McCullough
Tim Reid
PO Box 1500
Huntsville, AL 35807-3801

2 U. S. Army TACOM-ARDEC
SMCAR-AEE-WW
Attn: Ernest L. Baker
Chuck Chin
Picatinny Arsenal, NJ 07806-5000

2 Washington State University
Department of Physics
Shock Dynamics Laboratory
Attn: James R. Asay
Yogendra M. Gupta
Pullman, WA 99164-2814

2 Wright Laboratory
Attn: Dan Brubaker
William Cook
Bruce C. Patterson
Eglin AFB, FL 32542-5434

1 NIMIC, NATO Headquarters
Attn: Peter R. Lee
B-1110 Brussels
BELGIUM

1 M. W. C Dharma-wardana
National Research Council
Ottowa
CANADA K1A 0R6

1 University of British Columbia
Attn: Andrew Ng
Department of Physics & Astronomy
6224 Agricultural Road

Vancouver, BC V6T 1Z1
CANADA

1 Groupe d'Astrophysique (CNRS)
Attn: G. Chabrier
Ecole Normale Supérieure
46 Alée d'Italie
68364 Lyon Cedex 07
FRANCE

2 Commissariat à l'Energie Atomique
Centre d'Etudes de Bruyères-le-Châtel
Attn: Philippe Arnault
Dominique Gilles
BP 12, F91680 Bruyères-le-Châtel
FRANCE

1 Commissariat a l'Energie Atomique
Attn: Jean-Paul Plotard
Coutry, 77181
FRANCE

1 French German Research Institute (ISL)
Attn: Lionel Bourne
5, Rue de General Cassagnon
Saint-Louis Cedex, 68301
FRANCE

1 Institut für Physik
Humbolt-Universität zu Berlin
Attn: Dieter Beule
Invalidenstraße 110
D-10115 Berlin
GERMANY

1 Fachbereich Physik
Universität Rostock
Attn: Ronald Redmer
Universitätsplatz 3
D-18051 Rostock
GERMANY

1 Bhaba Atomic Research Center
High Pressure Physics Division
Attn: S. K. Sikka
Bombay - 400 085
INDIA

1 National Institute for Research
Attn: Toshi Sekine
Inorganic Materials, Namiki 1-1
Tsuhuba, Ibaraki 305-0044
JAPAN

1 Weizmann Institute of Science
Attn: Zeev Zinamon
Rehovot
ISRAEL

1 Yehuda Partom
Rafael, Box 2250
Haifa, 31021
ISRAEL

1 Institute of Chemical Physics
Attn: A. N. Dremin
Russian Academy of Sciences
Moscow, 142432
RUSSIA

2 Institute for High Energy Densities
Russian Academy of Sciences
Attn: V. E. Fortov
I. V. Lomonosov
Izhorskaya ul. 13/19
Moscow, 127412
RUSSIA

1 Russian Federal Nuclear Center
Attn: V. I. Tarzhanov
P.O. Box 245
Snezhinsk, Chelyabinsk 456770
RUSSIA

1 Russian Federal Nuclear Center
Attn: R. F. Trunin
Sarov, Nizhni Novgorod Region 607190
RUSSIA

1 Manfred Held
c/o Messerschmitt-Bölkow-Blohm
GmbH AG
Postfach 1340
Schrobenhausen, 8898
GERMANY

1 M. Musella
European Commission
Joint Research Centre
European Inst. for Transuranium Elements

7615 Karlsruhe
GERMANY

2 AWE
Attn: John Maw
Peter Thompson
Aldermaston, Reading
Berkshire R57 4PR
UNITED KINGDOM

1 MS 0316 J. B. Aidun, 9235
1 0318 P. Yarrington, 9230
1 0751 R. M. Brannon, 6117
1 0819 A. C. Robinson, 9231
1 0819 R. M. Summers, 9231
1 0819 T. G. Trucano, 9211
1 0819 M. K. Wong, 9231
1 0820 P. Chavez, 9232
1 0820 A. V. Farnsworth, 9232
1 0820 M. E. Kipp, 9232
1 0820 S. A. Silling, 9232
1 0820 P. A. Taylor, 9232
1 0834 A. C. Ratzel, 9110
1 0835 E. A. Boucheron, 9141
1 0836 E. S. Hertel, 9116
1 0836 D. Crawford, 9116
1 0836 R. G. Schmidt, 9116
1 0836 M. R. Baer, 9100
1 0836 M. Hobbs, 9116
1 1168 C. Deeney, 1646
1 1168 M. D. Furnish, 1647
1 1178 D. D. Bloomquist, 1630
1 1181 L. C. Chhabildas, 1647
1 1181 J. P. Davis, 1646
1 1181 C. A. Hall, 1647
1 1181 M. Knudson, 1646
1 1181 W. D. Reinhart, 1647
1 1181 T. F. Thornhill, 1647
1 1181 T. J. Vogler, 1647
1 1185 D. P. Kelly, 15417
1 1185 R. J. Dukart, 15417
1 1185 R. J. Weir, 15417
1 1186 M. P. Desjarlais, 1674
1 1186 R. J. Lawrence, 1674
1 1190 J. P. Quintenz, 1600
1 1191 Keith Matzen, 1670
1 1194 D. H. McDaniel, 1640
1 9042 J. J. Dike, 8743
1 9018 Central Technical Files, 8945-1
2 0899 Technical Library,9616